

An investigation of turbulent premixed counterflow flames using large-eddy simulations and probability density function methods

Ranjith R. Tirunagari^{a,*}, Stephen B. Pope^a

^a*Sibley School of Mechanical and Aerospace Engineering, Cornell University, Ithaca, NY 14853, USA*

Abstract

We report results from a coupled large-eddy simulation (LES)/probability density function (PDF) computational study of turbulent premixed flames in the Yale turbulent counterflow flame (TCF) burner. The Yale TCF burner in the premixed mode consists of two coaxial opposed nozzles: one emitting cold, fresh premixed reactants, $CH_4/O_2/N_2$, and the other hot stoichiometric combustion products. This results in a turbulent premixed flame close to the mean stagnation plane. Four critical parameters are identified in the experiments, namely, the bulk strain rate, the turbulent Reynolds number, the equivalence ratio of the reactants mixture and the temperature of the hot combustion products. These are varied independently. In the conditional statistics approach, the instantaneous centerline profiles of OH mass fraction and its gradient are used to identify (i) the interface between the two counterflowing streams referred to as the gas mixing layer interface (GMLI), and (ii) the turbulent flame front using a binary reaction progress variable, c . The conditional mean of the progress variable conditioned on distance Δ from the GMLI, $\langle c | \Delta \rangle$, and the PDF of the GMLI-to-flame-front distance, Δ_f , are used to quantify the effects of the critical parameters on the interactions of the turbulent premixed flame with the counterflowing hot combustion products, both in the experiments and in the simulations. The LES/PDF simulations are performed in a cylindrical domain between the two nozzle exit planes. A base case simulation involving reference values of the critical parameters is simulated, and the centerline profiles (both unconditional and conditional) of the velocity statistics and the mean progress variable are found to match well with the experimental data. Additionally, the LES/PDF simulations predict the experimentally-observed trends of the effects of the critical parameters on the turbulent premixed flame very well. More importantly, the probability of localized extinction at the GMLI (i.e., $1 - \langle c | \Delta = 0 \rangle$) and the PDF of the separation distance between the GMLI and flame front, Δ_f , compare well with the experiments for all the flow conditions explored in the parametric study. Three independent key quantities are computed from the LES/PDF simulations of the base case to examine if the simulations can be considered to be in the direct numerical simulation (DNS) limit. They are (i) the ratio of the resolved turbulent diffusivity to the resolved molecular diffusivity, \tilde{D}_T/\tilde{D} , (ii) the normalized mixing rate, Ω_{RTL} , and (iii) the normalized grid spacing, h/δ_L . The ratio of \tilde{D}_T/\tilde{D} is sufficiently small (≤ 0.02) and the value of Ω_{RTL} is sufficiently large (≈ 22) to be considered to be in the DNS limit. However, the ratio of h/δ_L is too large (≈ 0.6) and hence the LES/PDF cannot be considered to be in the DNS limit by this criterion. In spite of the poor spatial resolution, the particle-mesh method yields a flame speed close to the laminar flame speed and this likely explains the success of the present LES/PDF calculations of the TCF premixed flame over the full range of critical parameters.

Keywords: Large-eddy simulation, Probability density function methods, Turbulent premixed counterflow flames, Gas mixing layer interface, Conditional statistics, Direct numerical simulation limit

*Corresponding author.

Email address: rrt38@cornell.edu (Ranjith R. Tirunagari)

1. Introduction

The understanding of the complex interactions between turbulence and chemical reactions is of fundamental importance to the design of efficient practical combustion devices. One way of understanding these turbulence-chemistry interactions is through modeling tools. However, for the modeling tools to be reliable and predictive, systematic validation of the underlying computational models with experiments is necessary.

Early experimental studies were performed on the turbulent opposed-jet configuration in isothermal, non-premixed and premixed modes to establish a framework for computational validation [1–4]. Following the initial work, turbulent counterflow flames (TCFs) have been considered as one of the benchmark configurations to study turbulence-chemistry interactions [5–9]. The TCF configuration has several features, which prove to be advantageous for experimentalists and modelers, such as: the stabilization of the flame and the achievement of high Reynolds number without pilot flames; the realization of a variety of combustion regimes from stable to local extinction/re-ignition; the compactness of the combustion region; and, the practical relevance of the configuration to industrial combustion devices, e.g., internal combustion engines and gas turbines [5]. Many collaborative works involving experimental and numerical investigations of turbulent counterflow flames have been performed (e.g., in Darmstadt, Imperial College and Yale burners) to test models for mixing, turbulence and chemical reactions [10–15]. High-fidelity large-eddy simulation (LES) coupled with mixture-fraction based formulations are commonly used for the computational studies [7, 11, 12, 14].

Probability density function (PDF) methods have been successfully used in combination with the large-eddy simulation technique to treat both turbulent non-premixed [16–18] and premixed flames [19–21]. The computational work presented here aims to study the turbulence-chemistry interactions in the premixed mode of the turbulent counterflow flames (TCFs) using large-eddy simulation/probability density function (LES/PDF) methodology [22–24]. Of particular interest in this work are the turbulent premixed flames experimentally studied in the Yale turbulent counterflow flame (TCF) burner by research groups at Sandia National Laboratories and at Yale University [25]. A series of experiments are conducted on the Yale TCF burner in its premixed mode at different flame conditions, which are obtained by identifying four critical parameters and varying them independent of each other.

The premixed mode of the Yale TCF burner consists of two coaxial nozzles placed at some distance apart, and carrying counterflowing streams of cold, fresh premixed reactants ($CH_4/O_2/N_2$) against hot stoichiometric combustion products. The four critical parameters identified in the experiments are: (i) the bulk strain rate based on the bulk velocity of the fresh premixed reactants stream and the distance between the two nozzles, (ii) the equivalence ratio of the fresh premixed reactants, (iii) the turbulent Reynolds number of the premixed reactants stream, and (iv) the temperature of the hot stoichiometric products stream. It is interesting to note that different turbulent premixed flame behaviors are observed for different operating conditions of the premixed mode [25]. The rich experimental data available for this mode enable us to assess the validity and accuracy of the underlying models used in the LES/PDF computational methodology through detailed comparisons using the analysis of conditional statistics. By studying the effects of the above mentioned critical parameters on the turbulent premixed flame, we aim to elucidate the complex interactions between the flow and the chemistry.

Therefore, the main goal of this computational study is to demonstrate and characterize the performance of LES/PDF methodology for this experimentally-studied turbulent premixed flame that exhibits a variety of combustion regimes which (i) have practical relevance for devices such as gas turbines and combustion engines, and (ii) are known to be challenging to predict.

The remainder of the paper is organized as follows. In Sec. 2, we describe the experimental configuration of the Yale TCF burner in the premixed mode with base-case values of the critical parameters, followed by a description on the experimental methods employed to vary them. We then explain the procedures followed in the experiments to detect (i) the gas mixing layer interface (GMLI) between the two counterflowing streams, and (ii) the flame region, in which the binary progress variable c has a value of unity. This is followed by a description of the analysis of conditional statistics based on the GMLI. In Sec. 3, the coupled LES/PDF methodology is described along with a brief description of the velocity inflow boundary conditions. The key parameters used in the LES/PDF code are also presented. In Sec. 4, the focus is on the parametric

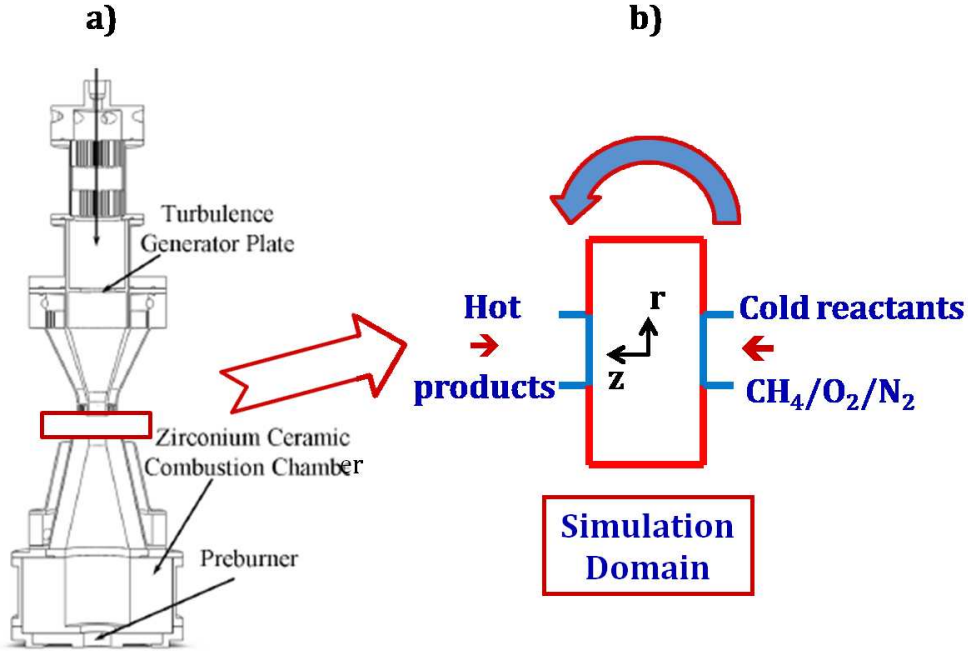


Figure 1: (a) The experimental configuration of the Yale TCF burner in the premixed mode and (b) the computational domain used in the LES/PDF simulations. The solution domain is taken as a cylindrical region between the two nozzle exit planes as highlighted by red box in (a). In the subsequent figures, the simulation results in the domain are shown such that the bottom stream (hot products) is on the left-hand side (LHS) and the top stream (cold reactants) is on the right-hand side (RHS). The computational domain aligns with the experimental configuration when it is rotated by 90° in the anti-clockwise direction as indicated by the arrow.

study of the critical parameters through the analysis of conditional statistics. Firstly, the simulation results on the centerline for the velocity and progress variable statistics are compared with the experimental data for the base case and subsequently, the parametric space is explored by quantifying the effects of the four critical parameters on the turbulent premixed flame through (i) the conditional mean of the progress variable conditioned on distance Δ from the GMLI as a function of Δ , $\langle c | \Delta \rangle$, and (ii) the PDF of the local separation between the GMLI and flame front, Δ_f . In Sec. 5, we examine the LES/PDF simulations of the base case in more detail by computing three independent key quantities to determine whether the LES/PDF simulations can be considered to be in the direct numerical simulation (DNS) limit. Finally, the conclusions from the study are summarized in Sec. 6.

2. Yale turbulent counterflow flame (TCF) burner in the premixed mode

2.1. Experimental configuration

The experimental study on the Yale turbulent counterflow flame (TCF) burner in the premixed mode are conducted at Sandia National Laboratories and at Yale University [25]. The influence of strain, reactants equivalence ratio, turbulence level, and mixing with counterflowing hot combustion products on the turbulent premixed flame is systematically investigated. In this sub-section, we describe the experimental configuration for the base-case values of the critical parameters.

Figure 1(a) shows the experimental configuration of the counterflow burner in the premixed mode in which two coaxial opposed nozzles of diameter $d_{jet} = 12.7$ mm are placed at a distance $d = 16$ mm apart. The computational domain used in the LES/PDF simulations is shown in Fig. 1(b). The top stream is a

Table 1: Reference values of the critical parameters in the base case.

Parameter	Reference value
K_{bulk} (1/s)	1400
ϕ_u	0.85
Re_t	1050
T_b (K)	1850

highly-turbulent reactants stream of a premixed $CH_4/O_2/N_2$ mixture at a turbulent Reynolds number of $Re_t = 1050$ with an equivalence ratio of $\phi_u = 0.85$ at unburnt temperature $T_u = 294$ K and pressure 1 atm. The turbulence in the top stream is generated by placing a turbulence generating plate (TGP) inside the nozzle [26]. The molar ratio of O_2/N_2 is fixed at 30:70 in this stream. The bottom nozzle hosts a pre-burner which burns stoichiometric $CH_4/O_2/N_2$ mixture to completion, so the bottom stream is a stream of hot stoichiometric combustion products with a measured temperature of $T_b = 1850$ K and 1 atm. The TGP is omitted in the bottom nozzle due to increased viscosity of the burnt combustion products. A turbulent premixed flame is then established near the stagnation plane between the two nozzles.

The bulk velocity in the upper jet is kept constant at $U_{bulk} = 11.2$ m/s. Based on U_{bulk} and d , the bulk strain rate K_{bulk} defined by

$$K_{bulk} = \frac{2U_{bulk}}{d}, \quad (1)$$

is 1400 1/s. The turbulent Reynolds number Re_t is defined as

$$Re_t = \frac{u'l'}{\nu_{N_2}}, \quad (2)$$

where u' , l' and ν_{N_2} are the axial r.m.s. velocity, the longitudinal integral length scale, and the kinematic viscosity of N_2 at 294 K and 1 atm., respectively. In the experiments, u' and l' are measured on the centerline at a distance of 0.5 mm downstream of the top nozzle exit. The reference values of the critical parameters for the base case are summarized in Table 1.

2.2. Parametric study

A systematic parametric study was performed on the Yale TCF burner in the premixed mode to investigate the effects of the four critical parameters on the interactions of highly-turbulent premixed $CH_4/O_2/N_2$ flames with stoichiometric counterflowing hot combustion products. The four critical parameters that are identified and independently varied in the experiments are: (a) the bulk strain rate, K_{bulk} ; (b) the equivalence ratio of the cold, fresh premixed $CH_4/O_2/N_2$ mixture in the reactants stream, ϕ_u ; (c) the turbulent Reynolds number, Re_t ; and (d) the temperature of the hot stoichiometric combustion products stream, T_b . It is important to note that we observe different turbulent flame behavior, both qualitatively and quantitatively, for the various flame conditions obtained by considering different sets of the critical parameters.

Table 2 summarizes the range of the critical parameters and the experimental method employed to vary each parameter. The bulk strain rate defined in Eq. 1 is varied from 1400 1/s to 2240 1/s by varying the distance between the two nozzles d from 16 mm to 10 mm, while keeping the bulk axial velocity, U_{bulk} , in the top stream constant at 11.2 m/s. In this study, three values of K_{bulk} are considered, namely, 1400, 1720, and 2240 1/s.

Both lean and stoichiometric flames are studied by varying the equivalence ratio of the fresh premixed reactants from 0.5 to 1.0. The concentration of CH_4 is varied while keeping the molar ratio of O_2/N_2 at the same ratio of 30:70. The four values considered for ϕ_u are 0.5, 0.7, 0.85, and 1.0.

The turbulent Reynolds number Re_t defined in Eq. 2 is varied by changing the position of the TGP inside the top nozzle. In this study, we consider two values of Re_t , namely, 470 and 1050. It is observed in the experiments that the closer the TGP is to the top nozzle exit, the higher the turbulent intensities

Table 2: Range of the critical parameters in the parametric study of the premixed mode.

Parameter	Range	Quantity varied
K_{bulk} (1/s)	1400 – 2240	Distance between the two nozzles, d
ϕ_u	0.5 – 1.0	CH_4 concentration in the top nozzle
Re_t	470, 1050	Distance between the TGP and top nozzle exit
T_b (K)	1700 – 1950	Molar ratio of O_2/N_2 in the bottom nozzle

at the top nozzle exit. The value of 470 is achieved by positioning the TGP at 124 mm upstream of the nozzle exit, whereas a value of 1050 is achieved when the TGP is 94 mm upstream of the nozzle exit. The axial r.m.s. velocity and the longitudinal integral length scale are equal to $u' = 2.2$ m/s and $l' = 3.2$ mm, respectively, for $Re_t = 470$; and $u' = 3.9$ m/s and $l' = 4.1$ mm for $Re_t = 1050$ [25].

The final parameter considered is the measured temperature T_b of the hot combustion products stream from the bottom nozzle. The molar ratio of O_2/N_2 is increased from 21:79 to 30:70 to increase T_b from 1700 to 1950 K, while keeping the equivalence ratio of the premixed mixture entering the pre-burner, ϕ_b , constant at 1.0. The mass flow rate from the bottom nozzle is slightly adjusted for different values of T_b . The four values of T_b considered are 1700, 1800, 1850, and 1950 K. (Note that there is considerable heat loss to the burner, since T_b is hundreds of degrees below the adiabatic flame temperature.)

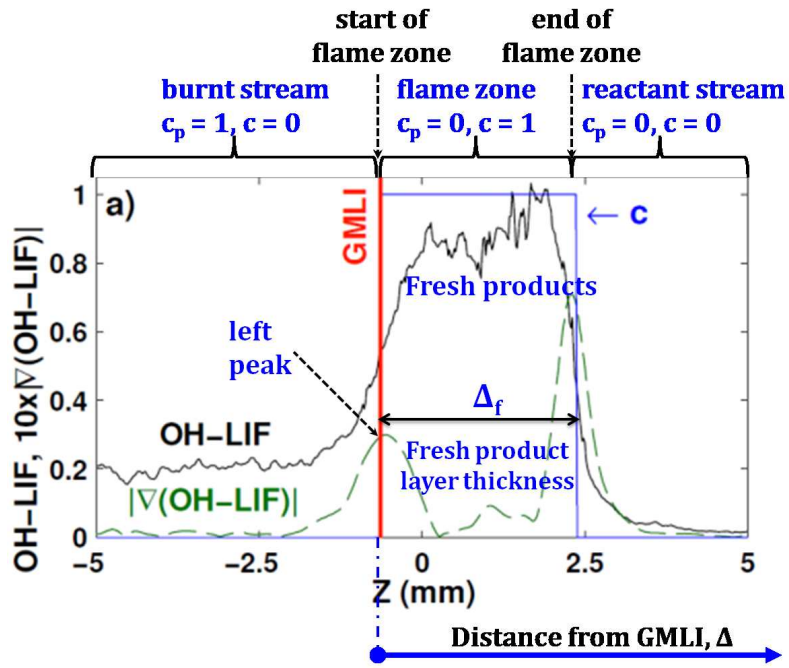
2.3. Conditional statistics

The procedure outlined in the experiments [25] for extracting conditional statistics is described in this subsection. The same procedure is followed in the computational work so as to compare the results from the LES/PDF simulations to the experimental data. In this method, the centerline profiles of the instantaneous OH mass fraction (obtained in the experiments using the OH-LIF signal) and its gradient are used to identify the gas mixing layer interface (GMLI) and the flame region as shown in Fig. 2. The centerline profiles are shown such that the hot products stream (i.e., burnt stream) is on the left-hand side (LHS) and the fresh reactants stream is on the right-hand side (RHS).

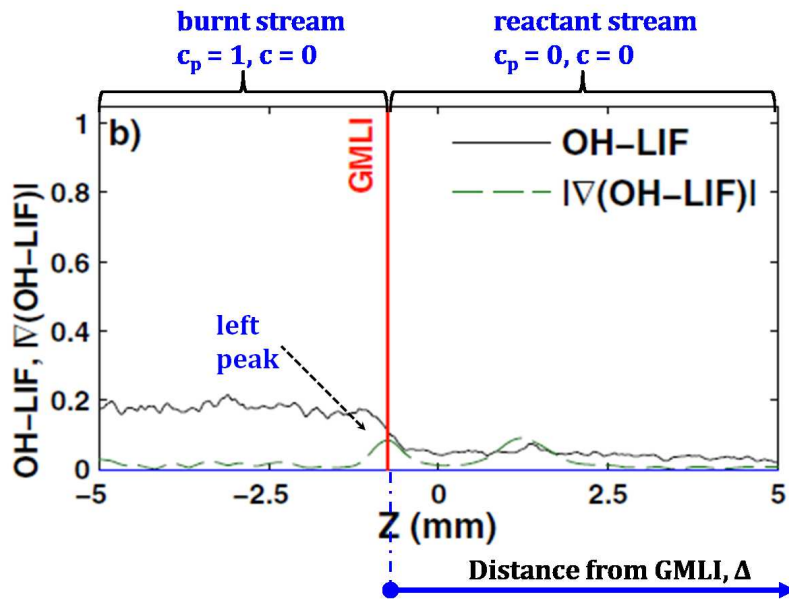
The GMLI is taken at the first peak in the $\nabla|(OH-LIF)|$ profile while traversing the profiles from left to right in Fig. 2. The GMLI signifies the boundary that separates the two opposed streams, namely, the burnt stream and the reactants stream. The flame region is identified as all pixels to the right of the GMLI that have a value of OH-LIF higher than a threshold value, which is taken to be moderately higher than the value observed in the burnt stream. A binary-valued progress variable, c , is introduced to track the fresh products from the turbulent flame front. It is taken to be equal to 1 in the flame region and 0 elsewhere. A similar binary variable c_p is used to represent the burnt stream. It has a value of 1 in the burnt stream and 0 elsewhere.

For the burning event (see Fig. 2(a)), we observe three distinct regions, namely, the burnt stream, the flame zone and the reactants stream. Note that the flame zone is on the reactants-stream side of the GMLI. For the extinguished event (see Fig. 2(b)), we observe only the burnt-stream and the reactants-stream regions, and the profile of OH-LIF drops from the observed value in the burnt stream to zero in the reactants stream without a peak. In the simulation, we use the centerline profiles of the resolved OH mass fraction in place of the OH-LIF signal.

The conditional statistics are formed in the reference frame attached to the GMLI. A local axial coordinate, Δ , is defined that is parallel to the burner centerline and has an origin that is coincident with the instantaneous GMLI. The separation distance between the GMLI and flame front (if it exists) is denoted by Δ_f . In the present analysis, two key conditional statistics are computed and analyzed. The first conditional statistic studied is the conditional mean progress variable $\langle c|\Delta \rangle$, which denotes the mean of c at a distance Δ from the GMLI. It also represents the probability of there being fresh combustion products at that location. At the GMLI (i.e., for $\Delta = 0$), c is unity for a burning event and zero for an extinguished event. Thus, $1 - \langle c|\Delta = 0 \rangle$ is the probability of localized extinction at the GMLI. The second conditional statistic studied is the probability density function (PDF) of the fresh product layer thickness, Δ_f . The



(a)



(b)

Figure 2: The centerline profiles of OH-LIF (black solid line) and $\nabla|OH-LIF|$ (green dashed line) for (a) a burning event and (b) an extinguished event. The instantaneous GMLI is the vertical line shown in red. The conditional statistics are based on the distance measured from the instantaneous GMLI location, i.e., Δ . The fresh product layer thickness is denoted by Δ_f , where the binary progress variable c is taken as 1. The burnt stream, flame zone and reactants stream are identified using the instantaneous centerline profiles of OH and its gradient. Note that the burnt stream is on the LHS, and the flame zone and the reactants stream are on the RHS of the GMLI. (Figure adapted from [25].)

fresh product layer thickness is also equal to the separation distance between the GMLI and the flame front. Note that the PDF is formed based only on burning events: Δ_f is zero for extinguished events.

3. LES/PDF methodology

The turbulent premixed counterflow flame is simulated using the LES/PDF methodology [22–24]. In this methodology, LES is used to represent the flow and turbulence, and the PDF method is used to represent the turbulence-chemistry interactions.

3.1. LES approach

The filtered LES transport equations for mass, momentum and scalars (resolved specific volume and mixture fraction) are solved on a structured grid in cylindrical coordinates by the low-Mach number, variable-density Navier-Stokes equation solver, NGA [27]. The turbulent viscosity is obtained by using the Lagrangian dynamic sub-grid scale model [28], and the same model is applied to the mixture fraction field to obtain the turbulent diffusivity. Thus, as functions of position \mathbf{x} and time t , the resolved fields determined by the LES are the velocity $\tilde{\mathbf{U}}(\mathbf{x}, t)$, the density $\tilde{\rho}(\mathbf{x}, t)$ and the turbulent diffusivity $\tilde{D}_T(\mathbf{x}, t)$.

3.2. Composition PDF method

In the usual numerical implementation of PDF methods [24], a large number of notional particles are distributed throughout the LES domain. Each particle carries information on its position, $\mathbf{X}^*(t)$, and composition, $\phi^*(t)$. The composition variable is a vector of length $n_s + 1$, consisting of specific mole numbers \mathbf{z} of the n_s chemical species and the mixture sensible enthalpy h_s . The particle/mesh code, HPDF [17], is employed to evolve the position and composition of each particle by solving a set of differential equations.

The particle position evolves based on the resolved velocity plus a random walk. The evolution equation for the position is given by the stochastic differential equation (SDE)

$$d\mathbf{X}^* = \left[\tilde{\mathbf{U}} + \frac{\nabla \tilde{\rho} (\tilde{D}_T + \tilde{D})}{\tilde{\rho}} \right]^* dt + \left[2 (\tilde{D}_T^* + \tilde{D}^*) \right]^{1/2} d\mathbf{W}, \quad (3)$$

where $\mathbf{W}(t)$ is an isotropic Wiener process and \tilde{D} is the resolved molecular diffusivity. The superscript ‘*’ denotes that the quantities are evaluated at the particle position, $(\mathbf{X}^*(t), t)$. As given by the second term on the RHS of Eq. 3, the effects of molecular transport are modeled as a random walk term in the particle position equation. This term is represented by the stochastic Wiener process and its magnitude is determined by the sum of the molecular and turbulent diffusivities.

The particle composition equation evolves by the ordinary differential equation (ODE)

$$\frac{d\phi^*}{dt} = -\Omega^* (\phi^* - \tilde{\phi}^*) + \mathbf{S}(\phi^*), \quad (4)$$

where, the first term on the RHS is the classical interaction by exchange with the mean (IEM) mixing model [29] and the second term is the reaction source term. Given the particle compositions, $\phi^*(t)$, the mean composition, $\tilde{\phi}$, is estimated at the cell centers. The IEM mixing model states that the particle composition, ϕ^* , relaxes to the mean composition interpolated onto the particle, $\tilde{\phi}^*$, at a specified mixing rate given by

$$\Omega = C_m \frac{\tilde{D}_T + \tilde{D}}{\Lambda^2}, \quad (5)$$

where the model constant $C_m = 4.0$ and Λ is the filter width in LES (usually denoted by Δ). The molecular diffusivity is taken to be equal to the thermal diffusivity under the unity Lewis number assumption and obtained from CHEMKIN’s transport library.

The chemical mechanism used in the simulations is the 16-species augmented reduced mechanism (ARM1) for methane oxidation [30]. The in-situ adaptive tabulation (ISAT) procedure [31, 32] with an error tolerance ϵ_{tol} of 1×10^{-4} is used to calculate the reaction source term $\mathbf{S}(\phi^*)$ in the composition equation. A two-way coupling is established between the NGA and HPDF codes by solving an additional transport equation for the resolved specific volume \tilde{v} in NGA as described in [18, 33]. Additionally, the resolved grid velocities and transport properties are transferred from the LES code to the PDF code and in return, the species mass fractions and temperature are transferred from the PDF code to the LES code.

3.3. Velocity inflow boundary conditions

The computational domain employed in the LES/PDF simulations is shown in Fig. 1(b). It is taken as a cylindrical volume between the two nozzle exit planes, as opposed to a more commonly used large computational domain that extends upstream of the nozzle exit planes. This relatively small solution domain is chosen to focus on the combustion region between the two nozzles and to make the LES/PDF simulations less expensive.

The turbulence that the flame encounters is largely determined by the turbulence generating plate (TGP) housed inside the top nozzle and therefore the velocity inflow boundary conditions at the top nozzle exit plane are non-trivial. A separate LES is performed for a turbulent, non-reactive, opposed-jet flow using the ‘PsiPhi’ LES code [14] on a large computational domain, which also includes the regions inside the nozzles (i.e., upstream of the nozzle exit planes). The time series of the three components of the velocity at the nozzle exit planes are then recorded from the large-domain LES. The time series data at one of the nozzle exit planes are suitably transformed and used as velocity inflow boundary conditions at the top nozzle exit plane in the present simulations. The transformations are performed so as to match the mean and r.m.s. quantities of the axial and radial velocities, and the longitudinal integral length scale on the centerline, at the top nozzle exit plane in the simulations to those measured at a distance of 0.5 mm downstream of the top nozzle exit in the experiments. The transformation procedure is described in detail in [34].

The hot products stream is represented by a steady velocity field with only radial profiles of the mean axial and radial velocities (i.e., no fluctuations). This assumption is motivated by the absence of the TGP in the bottom nozzle and the large viscosity of the hot combustion products. The experimental data available at a distance of 3 mm downstream of the bottom nozzle exit plane are scaled to obtain the radial profiles of the mean velocities. The scaling for the mean axial velocity is performed so that the volume flow rate is matched to that of the experiments and the scaling for the mean radial velocity is performed so that the mean stagnation plane is near the mid-plane. The velocity boundary conditions treatment of the hot products stream is also discussed in detail in [34].

3.4. LES/PDF simulation parameters

Table 3 summarizes the key LES/PDF simulation parameters associated with the base case simulation (see Table 1). The bulk axial velocities in the fresh reactants stream (top nozzle) and hot combustion products stream (bottom nozzle) are 11.2 m/s and 38.2 m/s, respectively. The higher value for the low-density hot products stream is chosen to counterbalance the momentum of the high-density reactants stream such that the turbulent premixed flame is shifted near the mid-plane. The bulk Reynolds number Re is calculated based on the bulk axial velocity U_{bulk} in the reactants stream and the diameter of the nozzle d_{jet} as:

$$Re = \frac{U_{bulk} d_{jet}}{\nu_{N_2}}, \quad (6)$$

where, ν_{N_2} is the kinematic viscosity of N_2 at 294 K and 1 atm. Since the bulk velocity is kept constant in the experiments for all the cases, the bulk Reynolds number Re is constant at a value of about 9400.

The grid size used in the LES/PDF simulations is $96 \times 96 \times 32$ in the axial, radial and azimuthal directions, respectively, with a finest grid spacing in the axial direction of $h \approx 0.1$ mm. This grid size corresponds to a total number of LES grid cells of approximately 0.3M (where $1M = 10^6$) and a total of approximately 6M particles in the PDF code (with nominally 20 particles per LES cell). The simulations are run primarily

Table 3: Simulation parameters used in the base case simulation of the premixed mode.

Simulation parameter	Base case
Nozzle exit diameter (mm), d_{jet}	12.7
Distance between nozzles (mm), d	16
Solution domain: height, diameter (mm)	16, 60
Top stream	$CH_4/O_2/N_2$ ($\phi_u = 0.85$)
Bottom stream	hot combustion products
Bulk axial velocity in the streams ^a (m/s), U_{bulk}	11.2; 38.2
Bulk Reynolds number, Re	9400
Bulk strain rate (1/s), K_{bulk}	1400
Turbulent Reynolds number, Re_t	1050
Temperature of the streams ^a , (K)	294; 1850
Grid size ($z \times r \times \theta$)	$96 \times 96 \times 32$
Total number of cells, particles	0.3M, 6M
Computational wall-clock time (μs /cell/timestep), (NGA%-HPDF%)	~ 25 (30%-70%)

^a The numerical values are for the top and bottom streams, respectively.

on NICS Darter clusters using up to 48 cores. The total computational wall-clock time is approximately 25 μs /cell/timestep with the particle code consuming approximately 70% of the total computational time.

The LES/PDF base case simulation is advanced for a physical time of 0.03 s from its initial condition to reach the statistically-stationary state and to collect statistics. This physical time corresponds to at least 20 flow-through times, where one flow-through time is defined as the time taken for a fluid particle to travel the distance between the two nozzles d at the bulk velocity of 11.2 m/s. The average time step used is 1×10^{-6} s, which gives an average value of 0.3 for the Courant-Friedrichs-Lewy (CFL) number.

4. LES/PDF simulation results

4.1. Base case simulation

The turbulent premixed flame established in the region sandwiched between the two nozzle exits is visualized by looking at the contour plots of important quantities on a plane intersecting the computational domain through the center. Figure 3 shows the instantaneous contour plots of temperature, mass fractions of CO_2 , OH , and N_2 , respectively, from the base case simulation. The hot combustion products stream is on the LHS and the cold, fresh reactants stream is on the RHS. The turbulent premixed flame is identified by the OH mass fraction signal in the contour plot of Y_{OH} as shown in Fig. 3(c). Additionally, the simulations predict that the flame is stabilized near the reactants nozzle lip as we see strands of T and products near the lip in the contour plots of T and Y_{CO_2} (see Figs. 3(a) and (b)): this is also observed in the experiments [B. Coriton, private communication]. The mass fractions of the inert gas N_2 in the two counterflowing streams are different due to the difference in the equivalence ratios, as can be seen in Fig. 3(d).

Figure 4 compares the mean and r.m.s. axial and radial velocities on the centerline for the base case simulation with the experimental data. The mean axial velocity on the centerline matches well with the experimental data. Its value on the combustion products stream side at $z = -5$ mm reaches almost twice the magnitude compared to the value in the reactants stream at $z = 8$ mm. Moreover, the gradient of the mean axial velocity is larger on the combustion products stream side than on the reactants stream side. The r.m.s. velocities match well with the experiments on the reactants stream side and subsequently go to zero on the combustion products stream side (as imposed by the boundary conditions). The mismatch between the simulations and experiments is highest near the mean stagnation plane. The r.m.s. axial velocity is

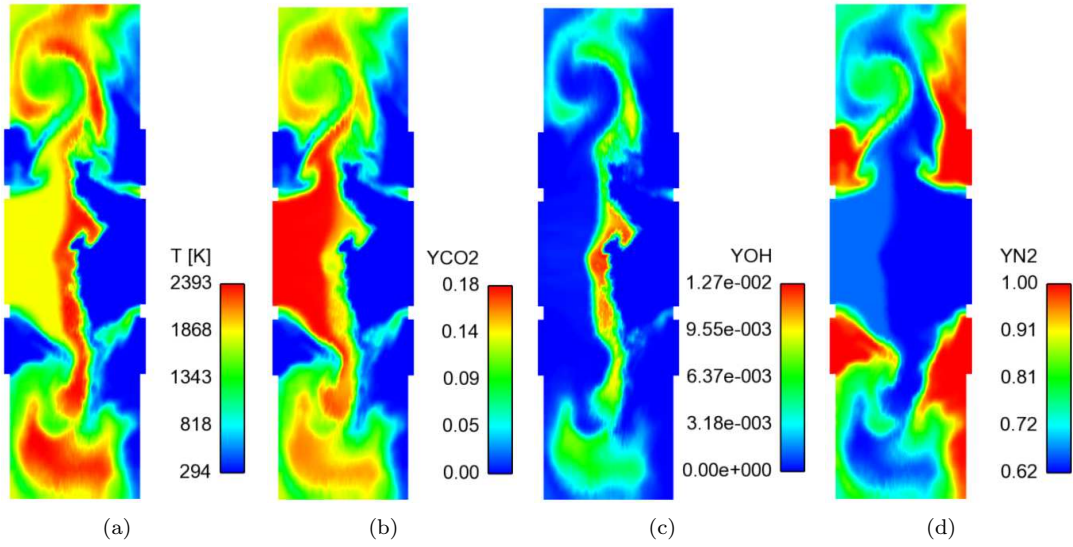


Figure 3: Instantaneous contour plots of (a) temperature, (b) CO_2 , (c) OH , and (d) N_2 mass fractions from the LES/PDF simulation of the base case (see Table 1) on a plane intersecting the solution domain through the center. The hot combustion products stream is on the LHS and the fresh reactants stream is on the RHS.

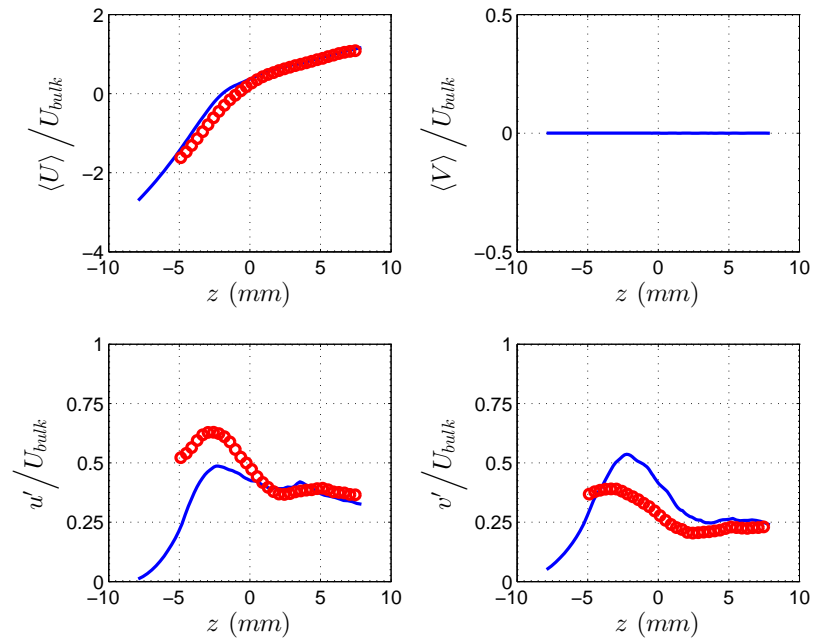


Figure 4: For the base case (see Table 1), the centerline profiles of the mean (top row) and r.m.s. (bottom row) axial and radial velocities; blue line: LES/PDF simulation, red symbols: experimental data [25]. The hot combustion products stream is on the LHS and the fresh reactants stream is on the RHS. The value of U_{bulk} is 11.2 m/s.

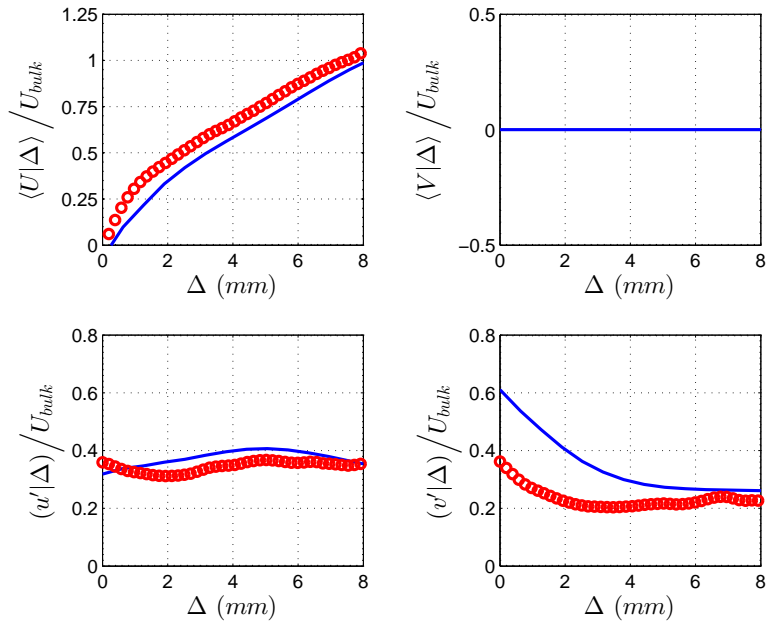


Figure 5: For the base case (see Table 1), the profiles of the conditional mean (top row) and r.m.s. (bottom row) axial and radial velocities as a function of distance Δ from the GMLI; blue line: LES/PDF simulation, red symbols: experimental data [25]. The value of U_{bulk} is 11.2 m/s.

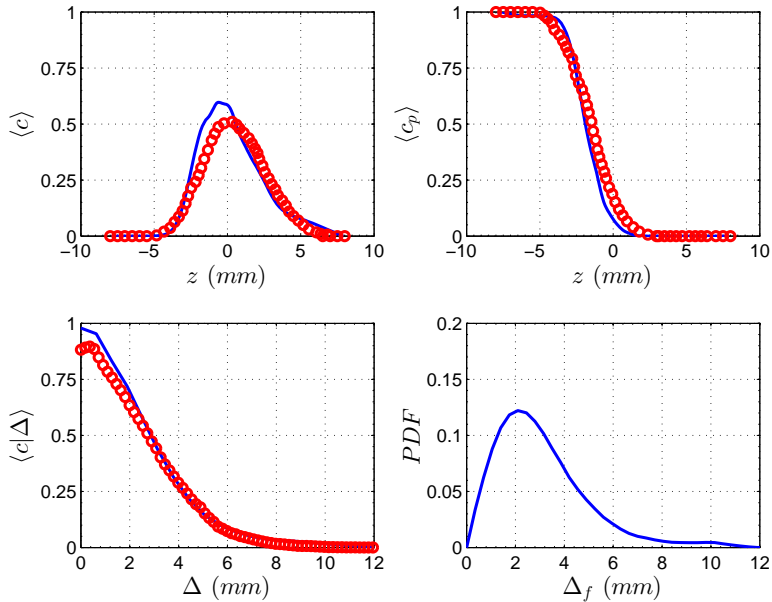


Figure 6: For the base case (see Table 1), (a) the profile of the mean progress variable $\langle c \rangle$ on the burner centerline (top left), (b) the profile of $\langle c_p \rangle$ on the burner centerline (top right), (c) the conditional mean progress variable $\langle c|\Delta \rangle$ as a function of distance Δ from the GMLI (bottom left), and (d) the PDF of the separation distance between the GMLI and the flame front, Δ_f (bottom right); blue line: LES/PDF simulation, red symbols: experimental data [25]. (There are no experimental data for the PDF of Δ_f for this case.)

under-predicted by about 25%, whereas the r.m.s. radial velocity is over-predicted by about 25% in the simulations. Both the r.m.s. quantities reach their respective maxima on the combustion products stream side in both the simulations and experiments.

Additionally, we compare the conditional mean and r.m.s. velocity profiles, conditioned on the distance Δ from the GMLI, with the experimental data as shown in Fig. 5. We infer from this figure that the simulation results match very well with the experimental data for the conditional mean axial velocity. An important observation can be made by considering the value of the conditional mean axial velocity at the location of the GMLI. The location of the GMLI is given by $\Delta = 0$ and the conditional mean axial velocity is zero at this location; therefore, the GMLI coincides with the mean stagnation plane. The gradient of the conditional mean axial velocity is larger at locations which are closer to the GMLI and smaller at locations away from the GMLI; this difference in the gradients is well predicted in the simulations. The conditional r.m.s. axial velocity is uniform as we move away from the GMLI (i.e., along the centerline towards the reactants stream); whereas the conditional r.m.s. radial velocity decreases sharply as we move away from the GMLI. The simulations predict the experimentally-observed trends well for both the fluctuation velocities, although the conditional r.m.s. radial velocity is over-predicted by nearly 50% at the GMLI location.

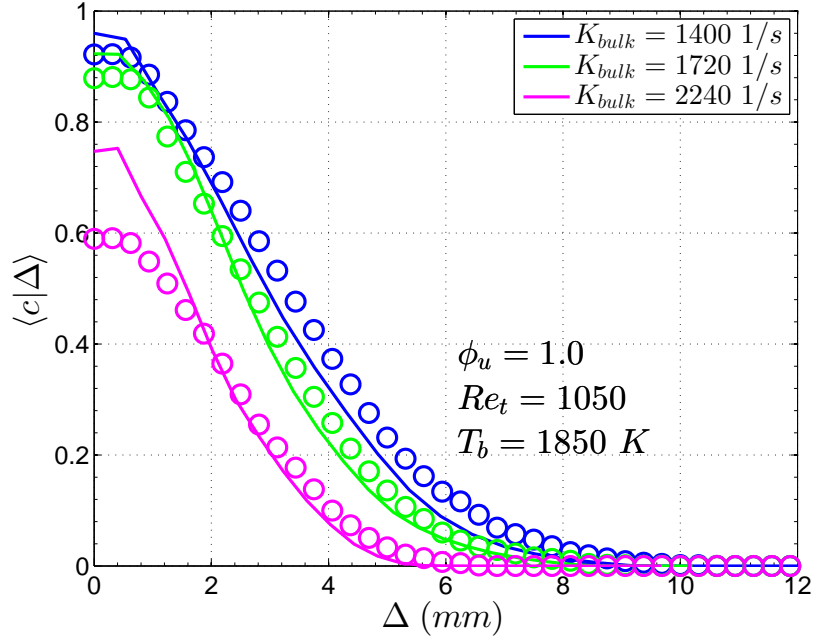
Finally, we consider the mean profiles of c and c_p on the centerline for the base case simulation, as shown in the top row of Fig. 6. The mean progress variable $\langle c \rangle$ gives the probability of finding fresh combustion products from the turbulent flame front. Similarly, the probabilities of finding gases from the products stream (bottom nozzle) and the reactants stream (top nozzle) are given by $\langle c_p \rangle$ and $1 - \langle c \rangle - \langle c_p \rangle$, respectively. Clearly, the simulations predict the experimental values well for both the profiles, for e.g., the probability of finding fresh products from the flame front at $z = 0$ mm is predicted to be 60% in the simulations, which is close to the value of 50% estimated in the experiments. The conditional mean progress variable conditioned on the distance Δ from the GMLI, $\langle c | \Delta \rangle$, and the PDF of the distance between the GMLI and the flame front (i.e., the thickness of the fresh product layer thickness), Δ_f , are plotted in the bottom row of Fig. 6. The simulations predict that there is a very low probability of localized extinction at the GMLI (i.e., $1 - \langle c | \Delta = 0 \rangle \approx 0$), however the measured probability in the experiments is about 10%.

4.2. Effect of bulk strain rate, K_{bulk}

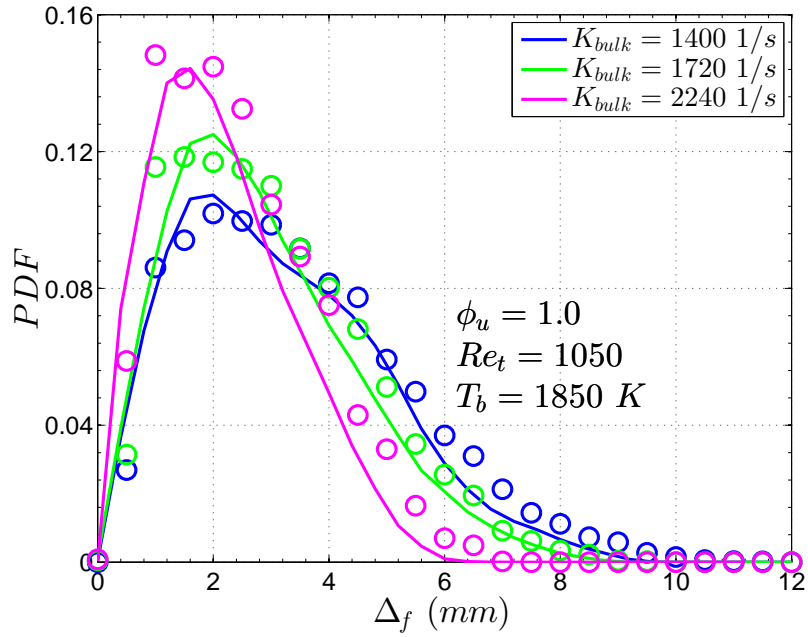
The response of the stoichiometric turbulent premixed flame is studied when the bulk strain rate K_{bulk} is increased from 1400 to 2240 1/s. In this study, the other critical parameters, namely, the turbulent Reynolds number Re_t , the reactants equivalence ratio ϕ_u and the products stream temperature T_b are kept constant at values of 1050, 1.0 and 1850 K, respectively. As shown in Fig. 7(a), the probability of localized extinction at the GMLI, given by $1 - \langle c | \Delta = 0 \rangle$, remains almost unchanged at about 10% (in both the simulations and experiments) when K_{bulk} is increased from 1400 1/s to 1720 1/s. However, a further increase in the bulk strain rate to 2240 1/s increases the probability of localized extinction to 40% in the experiments and to 24% in the simulations. As depicted in Fig. 7(b), the PDFs of the GMLI-to-flame-front distance, Δ_f , become narrow as the strain rate increases. We find good agreement between the simulation results and the experimental data for the two key quantities across the studied range of K_{bulk} .

4.3. Effect of reactants equivalence ratio, ϕ_u

To study the effect of reactants equivalence ratio on the turbulent premixed flame, we consider a range of values for this parameter from very lean ($\phi_u = 0.5$) to stoichiometry ($\phi_u = 1.0$), while keeping the values of K_{bulk} , Re_t and T_b constant at 1400 1/s, 1050 and 1850 K, respectively. Figure 8 shows that there is a good agreement between the simulation results and the experimental data. The probability of localized extinction at the GMLI increases as we decrease the equivalence ratio from 1.0 to 0.5 as shown in Fig. 8(a). The increase is most prominent for the $\phi_u = 0.5$ case. The probabilities of localized extinction in the simulations for $\phi_u = 1.0, 0.85, 0.7$ and 0.5 are approximately 4%, 4%, 24% and 84%, respectively. The corresponding experimental values are 8%, 10%, 40% and 85%, respectively. It can be observed from Fig. 8(b) that the peaks of the PDFs become narrow, and hence the flames move closer to the GMLI, as the flame becomes leaner.

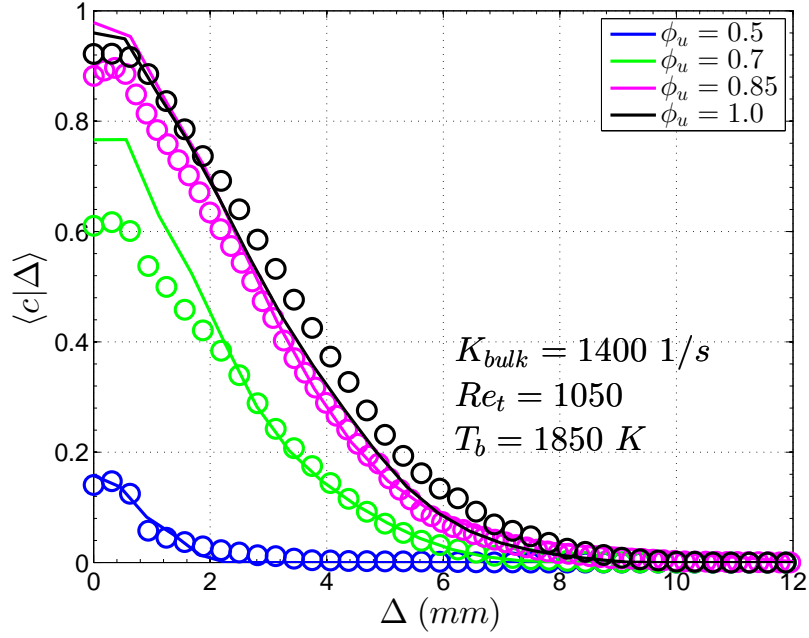


(a)

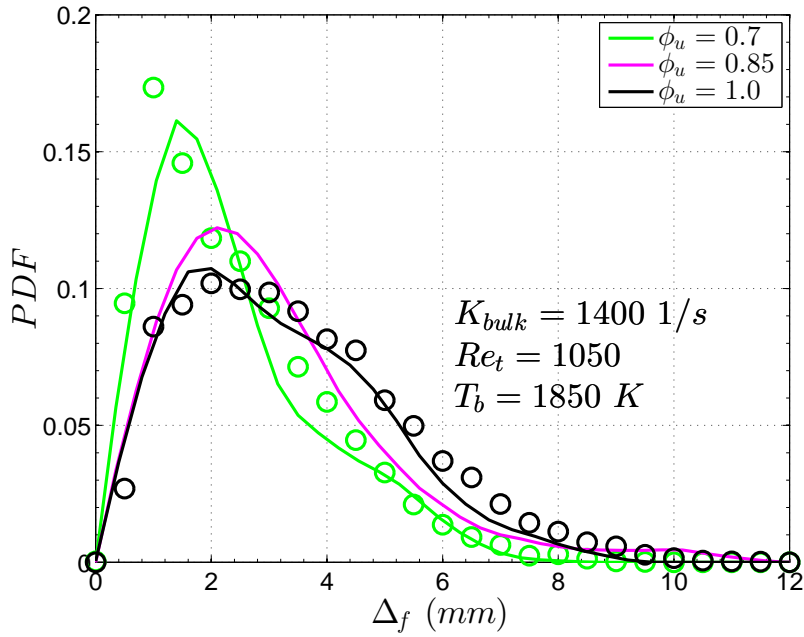


(b)

Figure 7: Effect of bulk strain rate K_{bulk} on the stoichiometric turbulent premixed flame ($\phi_u = 1.0$) at turbulent Reynolds number Re_t of 1050 and product stream temperature T_b of 1850 K. (a) Conditional mean progress variable as a function of distance Δ from the GMLI and (b) PDF of local separation between the GMLI and flame front, Δ_f ; lines: LES/PDF simulations, symbols: experimental data [25].

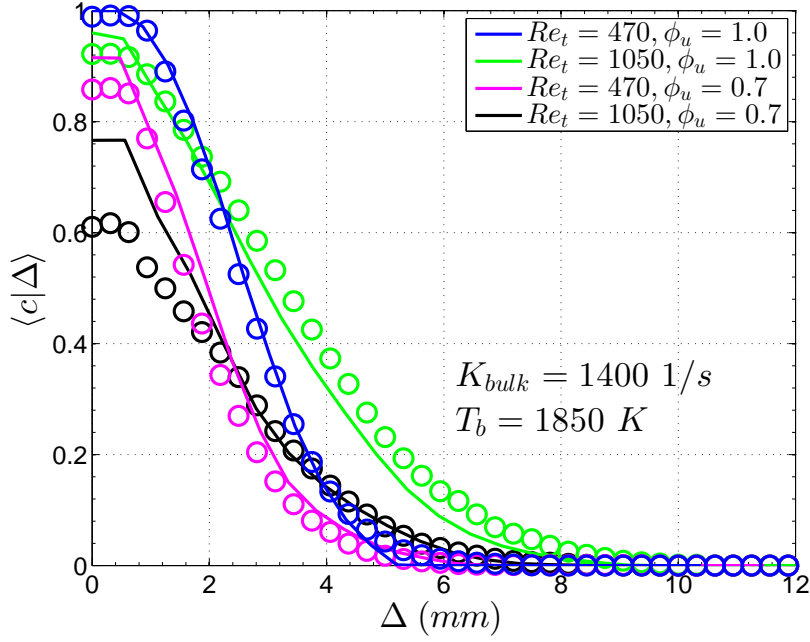


(a)

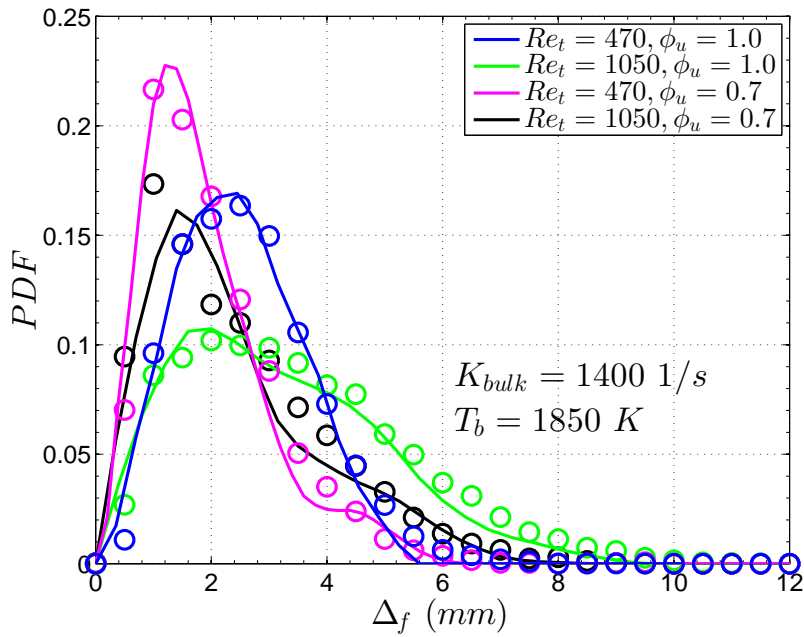


(b)

Figure 8: Effect of reactants equivalence ratio ϕ_u on the turbulent premixed flame at bulk strain rate K_{bulk} of 1400 1/s, turbulent Reynolds number Re_t of 1050 and product stream temperature T_b of 1850 K. (a) Conditional mean progress variable as a function of distance Δ from the GMLI and (b) PDF of local separation between the GMLI and flame front, Δ_f ; lines: LES/PDF simulations, symbols: experimental data [25].



(a)



(b)

Figure 9: Effect of turbulent Reynolds number Re_t on the stoichiometric ($\phi_u = 1.0$) and lean ($\phi_u = 0.7$) turbulent premixed flames at bulk strain rate K_{bulk} of 1400 1/s and product stream temperature T_b of 1850 K. (a) Conditional mean progress variable as a function of distance Δ from the GMLI and (b) PDF of local separation between the GMLI and flame front, Δ_f ; lines: LES/PDF simulations, symbols: experimental data [25].

4.4. Effect of turbulent Reynolds number, Re_t

Figure 9 show the effects of turbulent Reynolds number Re_t on the stoichiometric ($\phi_u = 1.0$) and lean ($\phi_u = 0.7$) turbulent premixed flames at $K_{bulk} = 1400$ 1/s and $T_b = 1850$ K. There is a good agreement between the simulations and experiments for both the flames. The stoichiometric flame at $Re_t = 470$ has the lowest probability of localized extinction with a unity value of $\langle c | \Delta = 0 \rangle$ in both the simulations and experiments. At the same value of Re_t , the lean flame has approximately 10% and 15% probabilities of localized extinction in the simulations and experiments, respectively. As we increase Re_t from 470 to 1050, the probabilities of localized extinction for the stoichiometric and lean flames in the simulations are approximately 8% and 24%, respectively. The corresponding values observed in the experiments are 10% and 40%, respectively. For both values of Re_t , we find that the peaks of the PDFs of the separation distance, Δ_f , for the lean flames are comparatively narrower as compared to the peaks for the stoichiometric flames. Therefore, the lean flame is in a more closer proximity to the GMLI as compared to the stoichiometric flame.

4.5. Effect of products stream temperature, T_b

To understand the effects of non-adiabaticity when the product stream temperature is below the adiabatic temperature, T_b is varied from 1950 to 1700 K for the stoichiometric ($\phi_u = 1.0$) and lean ($\phi_u = 0.7$) turbulent premixed flames at $K_{bulk} = 1400$ 1/s and $Re_t = 1050$. As shown in Fig. 10, the product stream temperature has negligible effect on the stoichiometric flame as the profiles of $\langle c | \Delta \rangle$ and the PDF of Δ_f overlap for different values of T_b . In contrast, the effect on the lean flame is more pronounced as shown in Fig. 11. When the product stream temperature T_b is decreased from 1950 to 1700 K, the probability of localized extinction increases and the PDF of Δ_f becomes slightly narrower for the lean flame. The simulations capture the contrasting effects of the product stream temperature T_b on the behavior of stoichiometric and lean turbulent premixed flames very well. The extinction probabilities predicted by the LES/PDF simulations for T_b values of 1700, 1800, 1850 and 1950 K for the lean flame are 96%, 80%, 24% and 16%, respectively. The corresponding values observed in the experiments are 96%, 80%, 40% and 24%, respectively. We also infer that the PDFs of the separation distance, Δ_f , are narrower for the lean flames as compared to that of the stoichiometric flames.

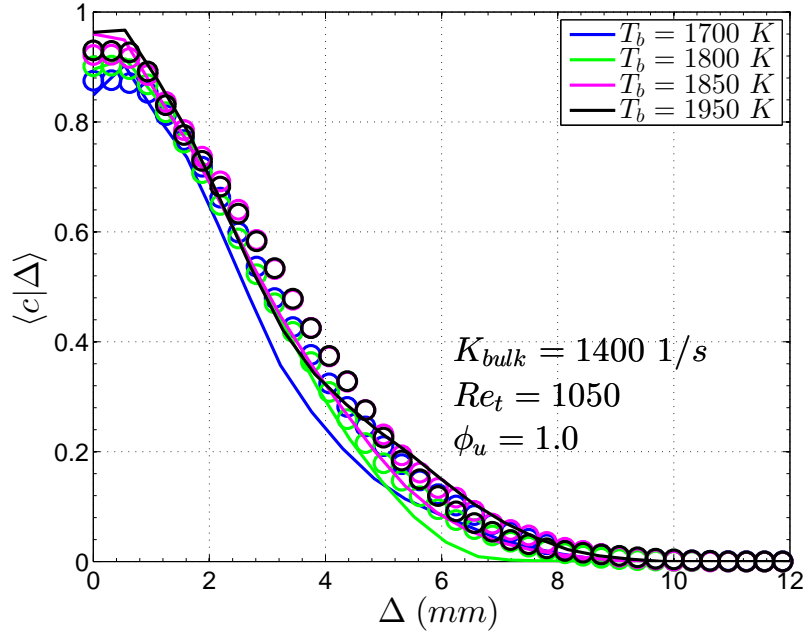
5. DNS limit consideration

In this section, we examine the LES/PDF simulations of the turbulent premixed flames in the Yale TCF burner in more detail by considering the base case simulation (see Table 1) as a representative example. In particular, three independent key quantities from the LES/PDF simulation of the base case are calculated and analyzed to determine if the simulations can be considered to be in the DNS limit.

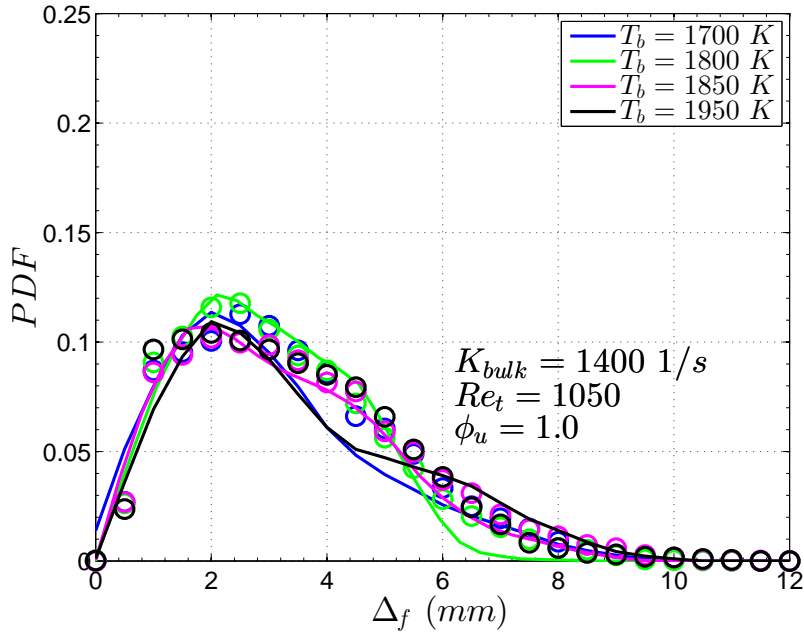
We denote the laminar flame speed and thickness by s_L and δ_L , the adiabatic flame temperature by T_a and the molecular diffusivity at the unburnt temperature T_u by D_u . The laminar-flame time scale τ_L is then defined as D_u/s_L^2 . The three quantities considered are:

1. The ratio of the resolved turbulent diffusivity to the resolved molecular diffusivity, \tilde{D}_T/\tilde{D} .
2. The normalized mixing rate, Ω_{RT_L} , where Ω_R is the value of the mixing rate Ω evaluated at temperature $T_R = \frac{1}{2}(T_a + T_u)$.
3. The ratio of the axial grid spacing on the centerline to the laminar flame thickness, h/δ_L .

In the DNS limit [35], the above quantities have the following limits: $\tilde{D}_T/\tilde{D} \rightarrow 0$, $\Omega_{RT_L} \rightarrow \infty$ and $h/\delta_L \rightarrow 0$. We now compare the centerline values of these quantities in the LES/PDF simulation of the base case to their corresponding values in the DNS limit. It is emphasized that all three quantities need to be sufficiently close to their respective DNS limits in order for the LES/PDF to be considered to be a DNS.

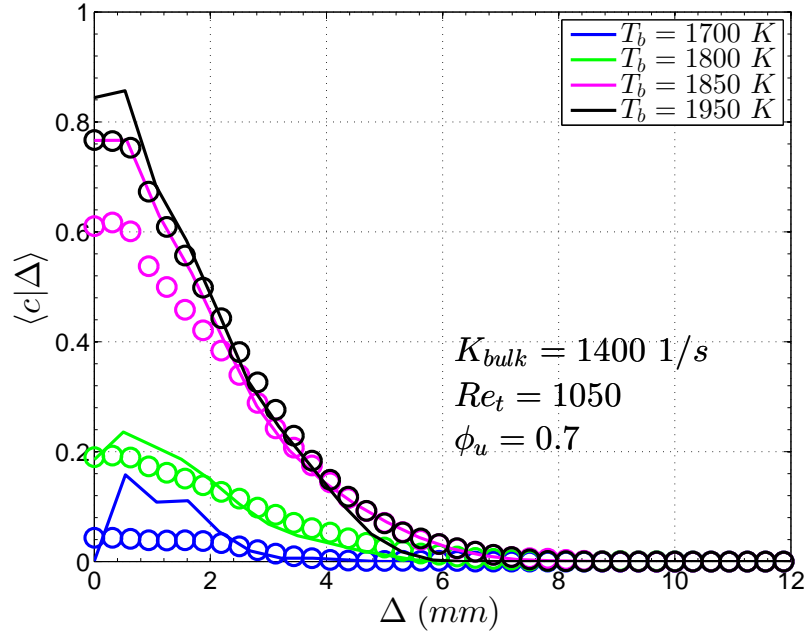


(a)

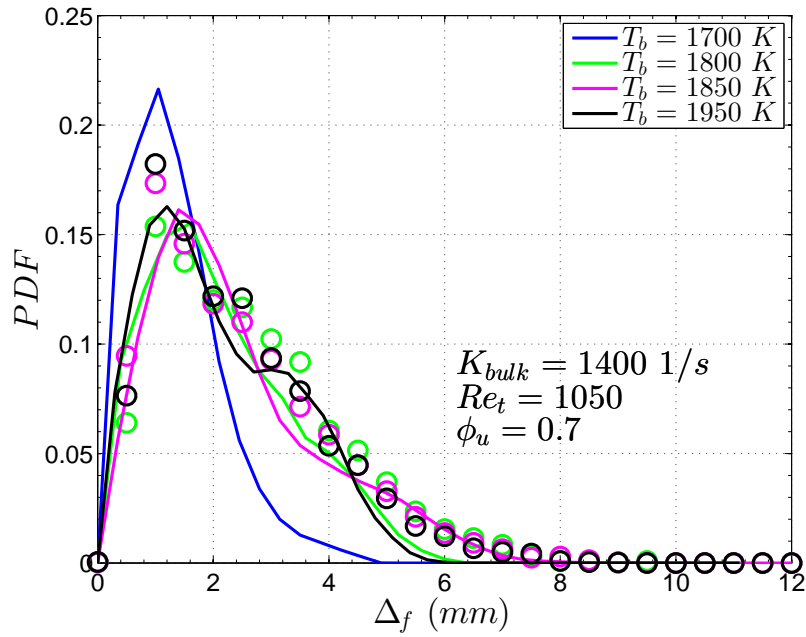


(b)

Figure 10: Effect of product stream temperature T_b on the stoichiometric ($\phi_u = 1.0$) turbulent premixed flame at bulk strain rate K_{bulk} of 1400 1/s and turbulent Reynolds number Re_t of 1050. (a) Conditional mean progress variable as a function of distance Δ from the GMLI and (b) PDF of local separation between the GMLI and flame front, Δ_f ; lines: LES/PDF simulations, symbols: experimental data [25].



(a)



(b)

Figure 11: Effect of product stream temperature T_b on the lean ($\phi_u = 0.7$) turbulent premixed flame at bulk strain rate K_{bulk} of 1400 1/s and turbulent Reynolds number Re_t of 1050. (a) Conditional mean progress variable as a function of distance Δ from the GMLI and (b) PDF of local separation between the GMLI and flame front, Δ_f ; lines: LES/PDF simulations, symbols: experimental data [25].

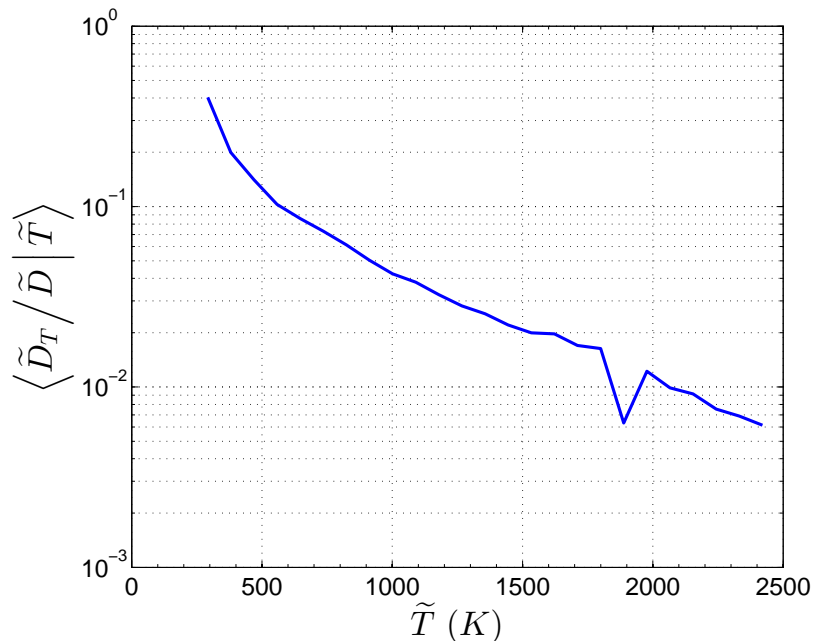


Figure 12: The conditional mean of the ratio of the resolved turbulent diffusivity to the resolved molecular diffusivity with respect to the resolved temperature on the centerline from the LES/PDF simulation of the base case (see Table 1).

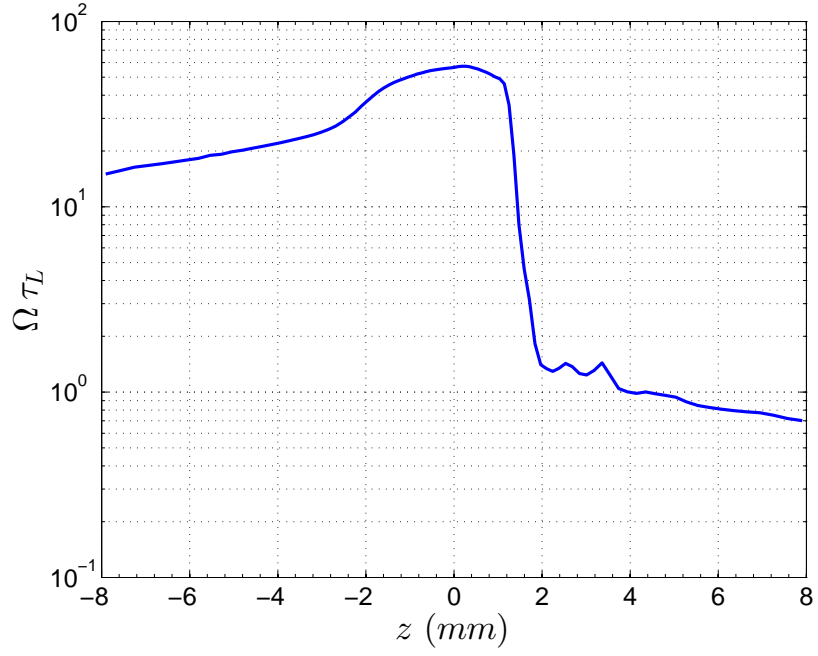
5.1. Laminar flame properties

To determine the laminar flame speed s_L and the adiabatic flame temperature T_a , the accurate solution to a one-dimensional, freely-propagating, unstrained, laminar premixed flame is obtained in CHEMKIN-PRO [36]. The laminar flame speed and adiabatic flame temperature of the premixed flame under $\phi_u = 0.85$ and $T_u = 294$ K is calculated to be $s_L = 56.6$ cm/s and $T_a = 2435$ K, respectively. Using the values of $D_u = 2.18 \times 10^{-5}$ m²/s and $s_L = 56.6$ cm/s, the laminar-flame time scale $\tau_L (= D_u/s_L^2)$ is calculated to be approximately 68 μ s. The temperature at which the mixing rate Ω is evaluated to compute the normalized mixing rate $\Omega_{R\tau_L}$ is given by $T_R = \frac{1}{2}(T_a + T_u) = 1365$ K.

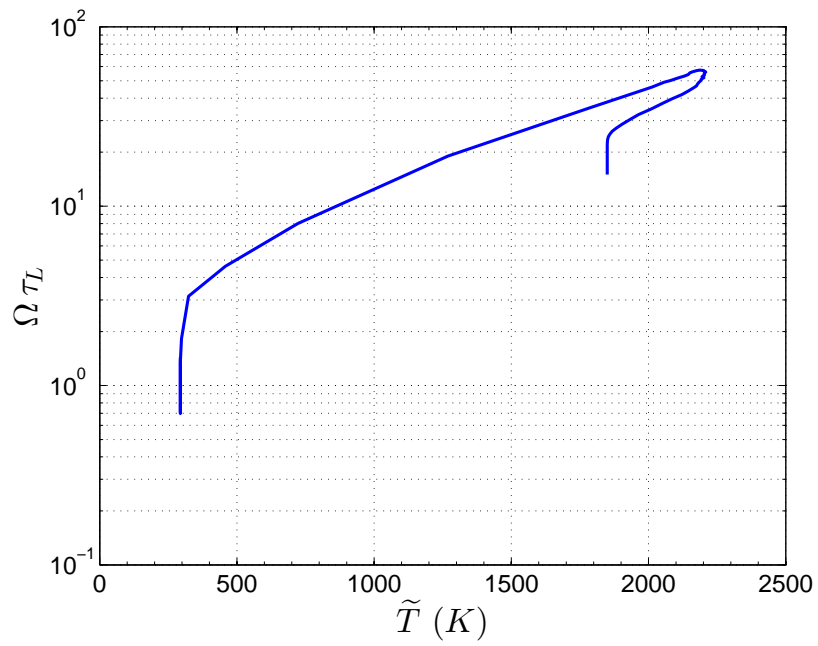
To compute the laminar flame thickness δ_L , a one-dimensional, strained, opposed-jet, laminar premixed flame with the streams compositions the same as those of the base case simulation is solved in CHEMKIN-PRO [36] to obtain the temperature profile on the centerline. We take the laminar flame thickness as the *secant thickness*, defined as follows. Let $x_{1/4}$ and $x_{3/4}$ denote the locations at which the normalized temperature $(T - T_u)/(T_{max} - T_u)$ has the values 1/4 and 3/4, respectively. Then we define the laminar flame thickness as $\delta_L = |2(x_{3/4} - x_{1/4})|$ and is found to be 0.25 mm.

5.2. Molecular diffusion

Figure 12 shows the conditional mean of \tilde{D}_T/\tilde{D} with respect to the resolved temperature \tilde{T} on the centerline for the base case simulation. The value of $\langle \tilde{D}_T/\tilde{D} | \tilde{T} \rangle$ is maximum at the temperature of the reactants stream and decreases as the temperature increases. We observe a dip in the profile at the products-stream temperature as the value of \tilde{D}_T is relatively small at the nozzle exit of the products stream. In regions of higher temperatures (for e.g., $\tilde{T} \geq 1500$ K), the premixed flame interacts with the counterflowing combustion products stream; and from Fig. 12, it can be inferred that in this region the value of $\langle \tilde{D}_T/\tilde{D} | \tilde{T} \rangle$ is at most 0.02. Roughly speaking, where combustion takes place, the turbulent diffusivity is less than 2% of the molecular diffusivity. Therefore, it can be concluded that the value of $\langle \tilde{D}_T/\tilde{D} | \tilde{T} \rangle$ is sufficiently small (for



(a)



(b)

Figure 13: Instantaneous plots of the centerline normalized mixing rate $\Omega \tau_L$ as a function of (a) distance between the two nozzles and (b) the centerline resolved temperature from the LES/PDF simulation of the base case (see Table 1)

$\tilde{T} \geq 1500$ K) to be considered to be in the DNS limit. We also note that the molecular diffusion plays a dominant role in defining the turbulence-chemistry interactions observed in the flame zone formed by the turbulent premixed flame in this opposed-jet configuration.

5.3. Mixing rate

The mixing rate Ω given by Eq. 5 is normalized by the laminar-flame time scale τ_L (see Sec. 5.1) to obtain the normalized mixing rate $\Omega\tau_L$. For the base case simulation, Fig. 13(a) shows an instantaneous plot of the normalized mixing rate $\Omega\tau_L$ on the centerline, and Fig. 13(b) shows the plot of the same quantity as a function of the centerline resolved temperature \tilde{T} (at the same instant). The normalized mixing rate is minimum in the reactants stream, increases as we approach the flame zone, and then decreases towards the products stream. From Fig. 13(b), the value of Ω_{RTL} at $T_R = 1365$ K for the base case simulation is approximately equal to 22. As now argued, this value is sufficiently large to be considered to be in the DNS limit.

The effect of the normalized mixing rate on the LES/PDF solutions is examined in a companion study [35], in which a mesh-free particle method is used to obtain numerically-accurate solutions for a freely propagating, one-dimensional, unstrained laminar flame. That study confirms that the observed flame speed u_F and thickness δ_F converge to the laminar-flame values (s_L and δ_L) as Ω_{RTL} tends to infinity. For the value $\Omega_{RTL} \approx 22$ of the current simulations, the flame speed and thickness are close to this limit, specifically $u_F/s_L = 1.04$ and $\delta_F/\delta_L = 1.09$. In contrast, at the smaller normalized mixing rate of $\Omega_{RTL} = 5$, there are significant departures of 28% and 48%, respectively, in u_F and δ_F . Thus, as far as the flame speed and thickness are concerned, we conclude that the normalized mixing rate $\Omega_{RTL} \approx 22$ is sufficiently large for the LES/PDF to be considered to be in the DNS limit by this criterion to a good approximation.

(In [35], the normalized mixing rate is expressed differently as a quantity denoted as $\Omega_u\tau_c$. The conversion between the two expressions of the normalized mixing rate is $\Omega_{RTL} = 16.5\Omega_u\tau_c$.)

A defect of the random-walk model of molecular diffusion is that it introduces spurious production of composition fluctuations. From the LES/PDF calculations of the unstrained laminar flame described in [35], it is found that for $\Omega_{RTL} \approx 22$, the maximum r.m.s. fluctuations in the reaction progress variable is 12%, and that it approaches zero slowly as $(\Omega_{RTL})^{-1/2}$.

Figure 14 shows an instantaneous scatter plot of the particle temperature *vs.* position on the centerline, color-coded by the particle mass fraction of OH from the LES/PDF simulation of the base case. The maximum r.m.s. of the normalized temperature $(T - T_u) / (T_a - T_u)$ is 35%. Evidently, $\Omega_{RTL} \approx 22$ is not sufficiently large for the fluctuations to be negligible, and hence by this criterion, the LES/PDF are not in the DNS limit.

5.4. Grid spacing

Figure 15 shows the centerline profiles of the instantaneous resolved temperature \tilde{T} at different instants of time from the LES/PDF simulation of the base case for $-4 \leq z \leq 4$. As can be seen from this figure, the profiles of the resolved temperature \tilde{T} vary considerably due to the turbulence encountered by the premixed flame and therefore, the flame brush spans approximately the z values between -4 mm and 4 mm. We now consider the values of normalized grid spacing (h/δ_L) on the centerline and in particular, for $-4 \leq z \leq 4$, to determine if the grid is sufficiently fine to resolve the flame thickness.

Figure 16 shows the normalized grid spacing (h/δ_L) on the centerline in the LES/PDF simulation of the base case. For $-4 \leq z \leq 4$, the values of normalized grid spacing, h/δ_L , lie between 0.36 and 0.8. Therefore, we can infer that the grid is coarse by at least by a factor of 4 compared to that needed to resolve the laminar flame thickness, as conventionally, at least 10 grid points are needed within the laminar flame thickness.

In the companion study [35], the present LES/PDF methodology (both model and code) is used to make calculations of a mildly-strained laminar premixed flame in an opposed-jet configuration. These calculations are performed for a wide range of normalized grid spacings, h/δ_L , and this confirms that the laminar-flame speed and thickness are recovered on sufficiently fine meshes. However, for $h/\delta_L = 0.36$ and $h/\delta_L = 0.8$ (i.e., over the range of the current turbulent flame calculations) the observed flame thicknesses are $\delta_F/\delta_L = 1.5$ and 2.5, respectively. Hence, predictably, this grid spacing is too coarse to resolve the laminar flame at all

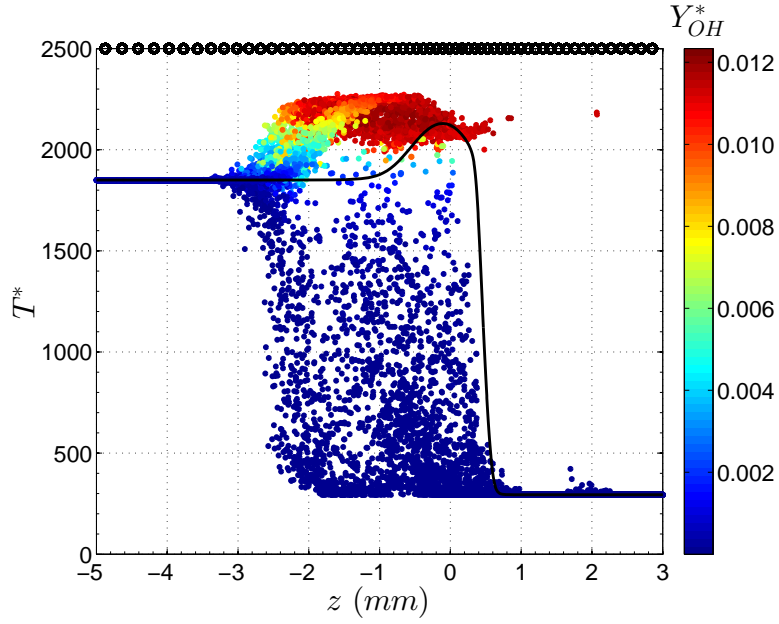


Figure 14: Scatter plot of the particle temperature on the centerline color-coded by the particle OH mass fraction from the LES/PDF simulation of the base case (see Table 1). The black solid line is the laminar profile from the solution of the strained, opposed-jet, laminar premixed flame (refer to Sec. 5.1). The grid points are shown as black circles on the top horizontal axis.

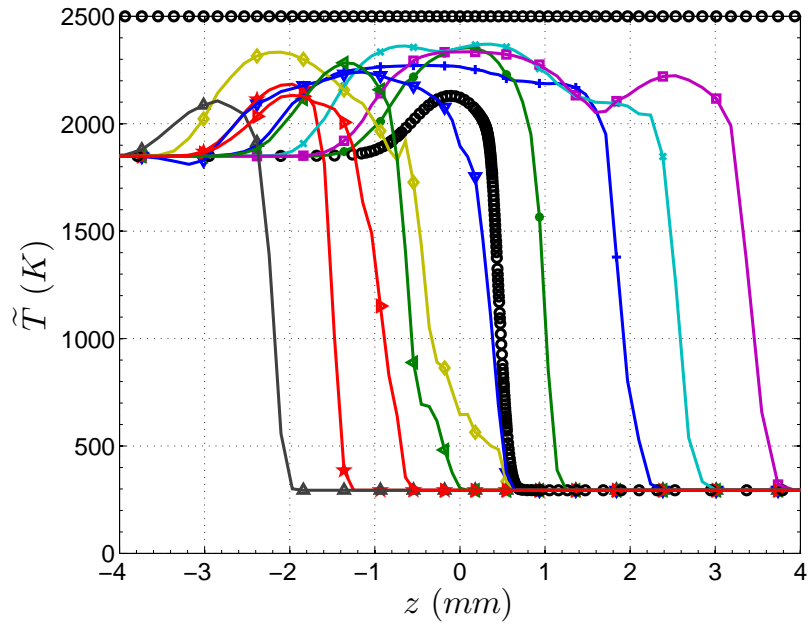


Figure 15: The centerline profiles of instantaneous resolved temperature \tilde{T} at different instants of time from the LES/PDF simulation of the base case (see Table 1). The black-symbols line is the laminar profile from the solution of the strained, opposed-jet, laminar premixed flame (refer to Sec. 5.1). The grid points are shown as black circles on the top horizontal axis.

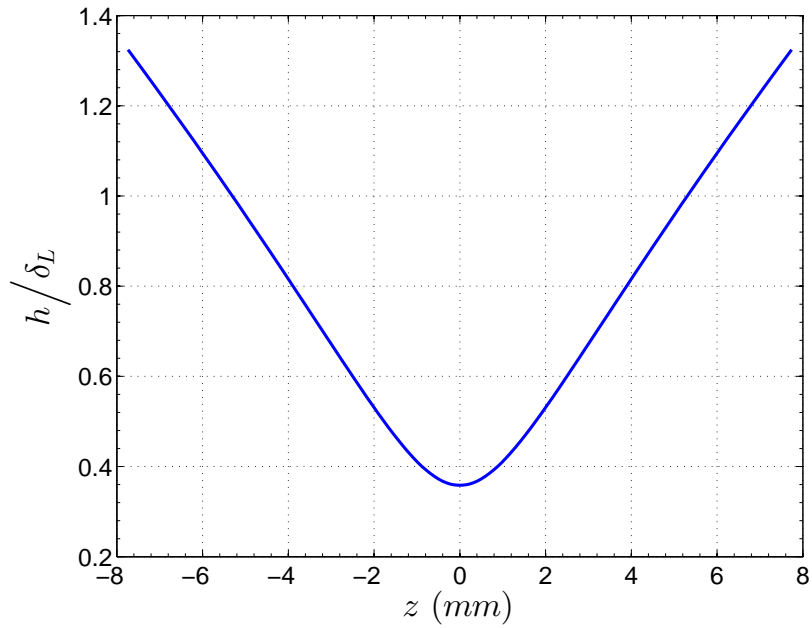


Figure 16: The normalized grid spacing on the centerline in the LES/PDF simulations of the base case (see Table 1).

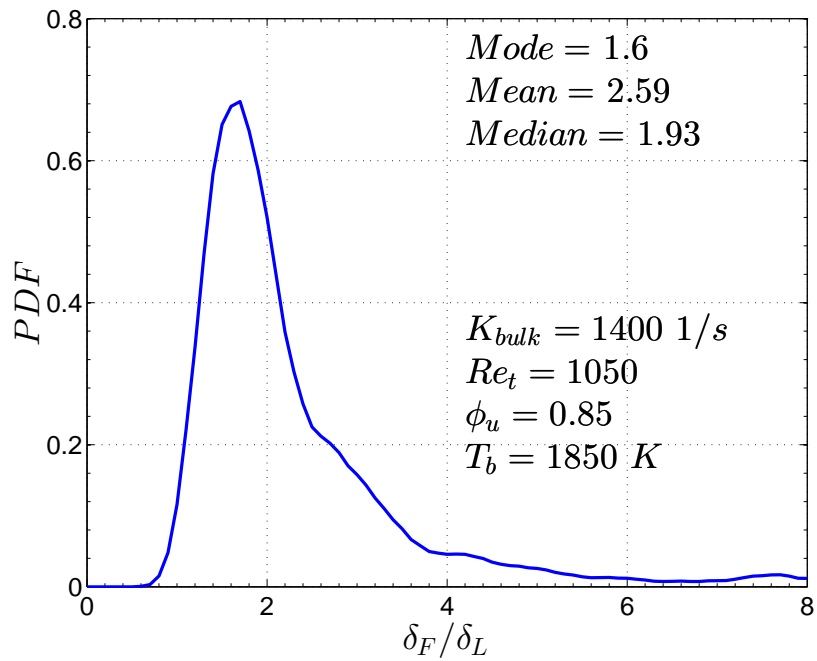


Figure 17: The PDF of the normalized flame thickness, δ_F/δ_L , calculated based on the centerline profiles of the resolved temperature \tilde{T} obtained from the LES/PDF simulations of the base case (see Table 1).

accurately, and consequently the present calculations are definitely not in the DNS limit. However, and this may be the key to the success of the present calculations, for h/δ_L in the range $[0.36, 0.8]$, the normalized flame speeds u_F/s_L observed in [35] are in the relatively narrow range $[0.7, 1.2]$ around unity.

Finally, we calculate the flame thickness based on the centerline profiles of the resolved temperature \tilde{T} (see Fig. 15) from the LES/PDF simulations of the base case. The flame thickness δ_F is calculated using the secant method at each instant of time. The PDF of the flame thickness δ_F normalized by the laminar flame thickness δ_L is shown in Fig. 17. The value of the mode signifies that there is a high probability that the observed flame thickness in the LES/PDF simulations is about 1.6 times the true laminar flame thickness. This value for the mode falls within the range (and closer to the lower limit) observed in the DNS limit study [35], i.e., $1.5 \leq \delta_F/\delta_L \leq 2.5$. Note that the flame thickness δ_F should not be confused with the fresh product layer thickness Δ_f . From Fig. 6, we observe that the mode of the PDF of Δ_f is close to 2 mm $\approx 8\delta_L \approx 16h$.

The conclusions from these considerations are summarized in items 9–14 in Sec. 6.

6. Conclusions

The following important conclusions can be drawn from the computational study presented in this paper:

1. The premixed mode of the Yale TCF burner is studied computationally using the LES/PDF methodology to examine the effects of four critical parameters (K_{bulk} , Re_t , ϕ_u and T_b) on the interactions of the turbulent premixed counterflow flame with the counterflowing combustion products.
2. A small cylindrical computational domain between the two opposed nozzle exits is employed for the computational study. The specification of the velocity inflow boundary conditions at the nozzle exit planes for the chosen computational domain is non-trivial. The inflow boundary condition method described in [34] is employed and found to be successful.
3. As in the experiments, the centerline profiles of OH mass fraction and its gradient are used to identify the gas mixing layer interface (GMLI) and the flame zone. The binary progress variable c is used to track fresh combustion products from the turbulent premixed flame.
4. The turbulence-chemistry interactions observed for different flame conditions, obtained by varying the identified critical parameters systematically, can be better understood by considering the mean profile of c conditioned on the distance Δ from the GMLI, i.e., $\langle c | \Delta \rangle$ and the PDF of the GMLI-to-flame-front distance (i.e., fresh product layer thickness), Δ_f .
5. For the base case simulation, the centerline profiles of the mean and r.m.s. axial and radial velocities and the mean progress variable match satisfactorily with the experimental data. Additionally, the conditional mean and r.m.s. axial and radial velocities and the conditional mean of the progress variable, conditioned on distance Δ from the GMLI, match well with the experimental data.
6. The LES/PDF simulations predict the experimentally-observed trends of the effects of the critical parameters very well, including the contrasting effects of the product stream temperature T_b on the stoichiometric and lean turbulent premixed flames.
7. The comparisons of the simulation results with the available experimental data for the two key quantities, i.e., $\langle c | \Delta \rangle$ and the PDF of Δ_f , are found to be successful for all the flame conditions obtained by varying the critical parameters systematically.
8. Three independent key quantities, namely, \tilde{D}_T/\tilde{D} , $\Omega_R\tau_L$ and h/δ_L , are extracted from the combustion zone of the LES/PDF simulations of the base case to determine whether the LES/PDF simulations can be considered to be in the DNS limit.
9. The ratio of turbulent-to-molecular diffusivity, \tilde{D}_T/\tilde{D} , is no larger than 0.02, and is thus small enough to be considered to be in the DNS limit.
10. The normalized mixing rate $\Omega_R\tau_L \approx 22$ is sufficiently large that accurate numerical simulations yield flame speeds and thicknesses within 4% and 9%, respectively, of their laminar values. To this extent, $\Omega_R\tau_L$ may be considered large enough to be in the DNS limit.

11. The previous point notwithstanding, because of the spurious production of fluctuations by the random walk model for molecular diffusion, the LES/PDF method applied to a laminar flame incorrectly yields significant (12%) composition fluctuations. Even larger fluctuations are evident in the present turbulent flame calculations.
12. The ratio of the grid spacing to the laminar flame thickness $h/\delta_L \approx 0.6$ is too large, by about a factor of 4, compared to that required for numerically-accurate calculations. For this reason, the present LES/PDF simulations cannot be considered to be in the DNS limit.
13. In spite of the poor spatial resolution, the particle-mesh method yields flame speeds close to the laminar speed (i.e., $u_F/s_L \approx 0.92$). This observation likely explains the success of the present TCF calculations over the full range of critical parameters.
14. Because of the poor spatial resolution, the observed flame thickness is about twice the laminar value, i.e., $\delta_F \approx 2\delta_L \approx 4h$.

Acknowledgements

The authors thank Dr. B. Coriton for helping with the rich experimental data and insightful discussions. We also thank Dr. M. W. A. Pettit for providing the time series of velocity from LES simulations using the ‘PsiPhi’ code. We gratefully acknowledge the California Institute of Technology, the University of Colorado at Boulder and Stanford University for licensing the NGA code used in this work. The authors thank the University of Tennessee and Oak Ridge National Laboratory Joint Institute for Computational Sciences and Cornell University Center for Advanced Computing for providing the computational resources required to perform this work.

Funding

This research is funded by the U.S. Department of Energy, Office of Science, Office of Basic Energy Sciences under award number DE-FG02-90 ER14128. This work used the Extreme Science and Engineering Discovery Environment (XSEDE), which is supported by National Science Foundation grant number ACI-1053575.

References

- [1] L. W. Kostiuk, K. N. C. Bray, T. C. Chew, Premixed turbulent combustion in counterflowing streams, *Combust. Sci. and Tech.* 64 (1989) 233–241.
- [2] E. Mastorakos, A. M. K. P. Taylor, J. H. Whitelaw, Extinction and temperature characteristics of turbulent counterflow diffusion flames with partial premixing, *Combust. Flame* 91 (1992) 40–54.
- [3] L. W. Kostiuk, K. N. C. Bray, R. K. Cheng, Experimental study of premixed turbulent combustion in opposed streams. Part I–nonreacting flow field, *Combust. Flame* 92 (1993) 377–395.
- [4] L. W. Kostiuk, K. N. C. Bray, R. K. Cheng, Experimental study of premixed turbulent combustion in opposed streams. Part II–reacting flow field and extinction, *Combust. Flame* 92 (1993) 396–409.
- [5] G. Coppola, B. Coriton, A. Gomez, Highly turbulent counterflow flames: A laboratory scale benchmark for practical systems, *Combust. Flame* 156 (2009) 1834–1843.
- [6] A. Gomez, Highly turbulent counterflow flames: A laboratory-scale benchmark for turbulent combustion studies, *Tech. rep.*, Fall Technical Meeting of the Eastern States Section of the Combustion Institute (2011).
- [7] D. Geyer, A. Kempf, A. Dreizler, J. Janicka, Turbulent opposed-jet flames: A critical benchmark experiment for combustion LES, *Combust. Flame* 143 (2005) 524–548.
- [8] K. H. H. Goh, P. Geipel, R. P. Lindstedt, Lean premixed opposed jet flames in fractal grid generated multiscale turbulence, *Combust. Flame* 161 (2014) 2419–2434.
- [9] P. Geipel, K. H. H. Goh, R. P. Lindstedt, Fractal-generated turbulence in opposed jet flows, *Flow Turbul. Combust.* 85 (2010) 397–419.
- [10] D. Geyer, A. Dreizler, J. Janicka, A. D. Permana, J. Y. Chen, Finite-rate chemistry effects in turbulent opposed flows: comparison of Raman/Rayleigh measurements and Monte Carlo PDF simulations, *Proc. Combust. Inst.* 30 (2005) 711–718.
- [11] D. Geyer, A. Kempf, A. Dreizler, J. Janicka, Scalar dissipation rates in isothermal and reactive turbulent opposed-jets: 1-D-Raman/Rayleigh experiments supported by LES, *Proc. Combust. Inst.* 30 (2005) 681–689.
- [12] A. Kempf, H. Forkel, J. Y. Chen, A. Sadiki, J. Janicka, Large-eddy simulation of a counterflow configuration with and without combustion, *Proc. Combust. Inst.* 28 (2000) 35–40.

- [13] R. P. Lindstedt, D. S. Luff, J. H. Whitelaw, Velocity fields of fuel lean premixed turbulent opposed jet flames, *Proc. Combust. Inst.* 31 (2007) 1459–1466.
- [14] M. W. A. Pettit, B. Coriton, A. Gomez, A. M. Kempf, Large-eddy simulation and experiments on non-premixed highly turbulent opposed jet flows, *Proc. Combust. Inst.* 33 (2011) 1391–1399.
- [15] J. Eckstein, J. Y. Chen, C. P. Chou, J. Janicka, Modeling of turbulent mixing in opposed jet configuration: one-dimensional Monte Carlo probability density function simulation, *Proc. Combust. Inst.* 28 (2000) 141–148.
- [16] F. A. Jaber, P. J. Colucci, S. James, P. Givi, S. B. Pope, Filtered mass density function for large-eddy simulation of turbulent reacting flows, *J. Fluid Mech.* 401 (1999) 85–121.
- [17] H. Wang, S. B. Pope, Large-eddy simulation/probability density function modeling of a turbulent $\text{CH}_4/\text{H}_2/\text{N}_2$ jet flame, *Proc. Combust. Inst.* 33 (2011) 1319–1330.
- [18] Y. Yang, H. Wang, S. B. Pope, J. H. Chen, Large-eddy simulation/probability density function modeling of a non-premixed CO/H_2 temporally evolving jet flame, *Proc. Combust. Inst.* 34 (2013) 1241–1249.
- [19] I. A. Dodoulas, S. Navarro-Martinez, Large eddy simulation of premixed turbulent flames using the probability density function approach, *Flow Turbul. Combust.* 90 (2013) 645–678. doi:10.1007/s10494-013-9446-z.
- [20] J. Kim, S. B. Pope, Effects of combined dimension reduction and tabulation on the simulations of a turbulent premixed flame using large-eddy simulation/probability density function, *Combust. Theor. Model.* 18 (2014) 388–413.
- [21] S. B. Pope, R. Tirunagari, Advances in probability density function methods for turbulent reactive flows, in: *Proceedings of the Nineteenth Australasian Fluid Mechanics Conference*, RMIT University, Melbourne, 2014.
- [22] S. B. Pope, *Turbulent Flows*, Cambridge University Press, Cambridge, 2000.
- [23] H. Pitsch, Large-eddy simulation of turbulent combustion, *Annu. Rev. Fluid. Mech.* 38 (2006) 453–482.
- [24] S. B. Pope, PDF methods for turbulent reactive flows, *Prog. Energy Combust. Sci.* 11 (1985) 119–192.
- [25] B. Coriton, J. H. Frank, A. Gomez, Effects of strain rate, turbulence, reactant stoichiometry and heat losses on the interaction of turbulent premixed flames with stoichiometric counterflowing combustion products, *Combust. Flame* 160 (2013) 2442–2456.
- [26] G. Coppola, A. Gomez, Experimental investigation on a turbulence generation system with high-blockage plates, *Exp. Therm. Fluid Sci.* 33 (2009) 1037–1048.
- [27] O. Desjardins, G. Blanquart, G. Balarac, H. Pitsch, High order conservative finite difference scheme for variable density low mach number turbulent flows, *J. Comput. Phys.* 227 (2008) 7125–7159.
- [28] C. Meneveau, T. S. Lund, W. H. Cabot, A lagrangian dynamic subgrid-scale model of turbulence, *J. Fluid Mech.* 319 (1996) 353–385.
- [29] J. Villermaux, J. C. Devillon, Représentation de la coalescence et de la redispersion des domaines de ségrégation dans un fluide par un modèle d’interaction phénoménologique, in: *Proc. 2nd Int. Symp. Chem. React. Eng.*, Elsevier, New York, 1972, pp. 1–13.
- [30] C. J. Sung, C. K. Law, J. Y. Chen, An augmented reduced mechanism for methane oxidation with comprehensive global parametric validation, *Proc. Combust. Inst.* 27 (1998) 295–304.
- [31] S. B. Pope, Computationally efficient implementation of combustion chemistry using in situ adaptive tabulation, *Combust. Theor. Model.* 1 (1997) 41–63.
- [32] L. Lu, S. R. Lantz, Z. Ren, S. B. Pope, Computationally efficient implementation of combustion chemistry in parallel PDF calculations, *J. Comput. Phys.* 228 (2009) 5490–5525.
- [33] P. P. Popov, H. Wang, S. B. Pope, Specific volume coupling and convergence properties in hybrid particle/finite volume algorithms for turbulent reactive flows, *J. Comput. Phys.* 294 (2015) 110–126.
- [34] R. R. Tirunagari, M. W. A. Pettit, A. M. Kempf, S. B. Pope, A simple approach for specifying velocity inflow boundary conditions in simulations of turbulent opposed-jet flows, *Flow Turbul. Combust.*, submitted for publication. Preprint available at https://tcg.mae.cornell.edu/pubs/Tirunagari_PKP_FTC_2015.pdf.
- [35] R. R. Tirunagari, S. B. Pope, LES/PDF for premixed combustion in the DNS limit, *Combust. Theor. Model.*, submitted for publication. Preprint available at https://tcg.mae.cornell.edu/pubs/Tirunagari_P_CTM_2015.pdf.
- [36] R. J. Kee, F. M. Rupley, J. A. Miller, M. E. Coltrin, J. F. Grear, E. Meeks, H. K. Moffat, A. E. Lutz, G. Dixon-Lewis, M. D. Smooke, J. Warnatz, G. H. Evans, R. S. Larson, R. E. Mitchell, L. R. Petzold, W. C. Reynolds, M. Caracotsios, W. E. Stewart, P. Glarborg, C. Wang, O. Adigun, Chemkin collection, release 3.6, in: *Reaction Design*, Inc., San Diego, CA, 2000.